VLT/FORS2 Spectroscopy in the GOODS-South Field

The FORS2 instrument at the ESO VLT has been used to obtain spectra of a large sample of faint galaxies in the Chandra Deep Field South in the framework of the Great Observatories Origins Deep Survey (GOODS). A total of 303 objects with magnitude $z_{850} \leq 25.5$ has been observed, providing 234 redshift determinations. The reduced spectra and the derived redshifts are released to the community (http://www.eso.org/science/goods/). They constitute an essential contribution to reach the scientific goals of GOODS, providing the time coordinate needed to delineate the evolution of galaxy masses, morphologies, and star formation, calibrating the photometric redshifts that can be derived from the imaging data at 0.36–8 μm and enabling detailed studies of the physical diagnostics for galaxies in the GOODS field.

E. Vanzella[1],
S. Cristiani[1],
M. Dickinson[2],
H. Kuntschner[3],
L. A. Moustakas[4],
M. Nonino[1], P. Rosati[5],
D. Stern[7],
C. Cesarsky[5],
S. Ettori[5],
H. C. Ferguson[4],
R.A.E. Fosbury[3],
M. Giavalisco[4],
J. Haase[3], A. Renzini[5],
A. Rettura[5,6],
P. Serra[3],
and the GOODS Team

[1]INAF - Osservatorio Astronomico di Trieste, Italy
[2]National Optical Astronomy Obs., Tucson, Arizona
[3]ST-ECF, Garching, Germany
[4]Space Telescope Science Institute, Baltimore, USA
[5]European Southern Observatory,
[6]Université Paris-Sud 11, Orsay, France
[7]Jet Propulsion Laboratory, California Institute of Technology, Pasadena, USA

The Great Observatories Origins Deep Survey (GOODS) is a public, multi-facility project that aims to answer some of the most profound questions in cosmology: how did galaxies form and assemble their stellar mass? When was the morphological differentiation of galaxies established and how did the Hubble Sequence form? How did AGN form and evolve, and what role do they play in galaxy evolution? How much do galaxies and AGN contribute to the extragalactic background light? Is the expansion of the universe dominated by a cosmological constant? A project of this scope requires large and coordinated efforts from many facilities, pushed to their limits, to collect a database of sufficient quality and size for the task at hand. It also requires that the data be readily available to the worldwide community for independent analysis, verification, and follow-up.

The program targets two carefully selected fields, the Hubble Deep Field North (HDF-N) and the Chandra Deep Field South (CDF-S), with three NASA Great Observatories (HST, Spitzer and Chandra), ESA's XMM-Newton, and a wide variety of ground-based facilities. The area common to all the observing programs is 320 arcmin^2, equally divided between the North and South fields. For an overview of GOODS, see Dickinson et al. (2003), Renzini et al. (2002) and Giavalisco et al. (2004a). Spectroscopy is essential to reach the scientific goals of GOODS. Reliable redshifts provide the time coordinate needed to delineate the evolution of galaxy masses, morphologies, clustering, and star formation. They calibrate the photometric redshifts that can be derived from the imaging data at 0.36–8 μm. Spectroscopy will measure physical diagnostics for galaxies in the GOODS field (e.g., emission line strengths and ratios to trace star formation, AGN activity, ionization, and chemical abundance; absorption lines and break amplitudes that are related to the stellar population ages). Precise redshifts are also indispensable to properly plan for future follow-up at higher dispersion, e.g., to study galaxy kinematics or detailed spectral-line properties.

The ESO/GOODS spectroscopic program is designed to observe all galaxies for which VLT optical spectroscopy is likely to yield useful data. The program makes full use of the VLT instrument capabilities (FORS2 and VIMOS), matching targets to instrument and disperser combinations in order to maximize the effectiveness of the observations. The magnitude limits and selection bandpasses depend to some degree on the instrumental setup being used. The aim is to reach mag ~24–25 with adequate S/N, with this limiting magnitude being in the *B*-band for objects observed with the VIMOS LR-Blue grism, in the *V*-band for those observed in the VIMOS LR-Red grism, and in the *z*-band for the objects observed with FORS2. This is not only a practical limit, however, but is also well matched to the scientific aims of the GOODS program. The ACS i_{775} imaging samples rest-frame optical (*B*-band) light out to $z = 1$, where $i_{775} = 25$ reaches 1.5 to 2 magnitudes past L^*_B This is also the practical limit for high-quality, quantitative morphological measurements from the ACS images (cf. Abraham et al. 1996). Similarly, $i_{775} = 25$ is ~1 mag fainter than the measured L^* UV for $z = 3$ Lyman Break Galaxies (LBGs), and 0.5 mag fainter than that at $z = 4$ (Steidel et al. 1999). These are the limits to which GOODS/SIRTF IRAC data will robustly measure rest-frame near-IR light, and hence constrain the stellar mass.

The Selection of the Targets for the FORS2 Spectroscopy

Objects were selected as candidates for FORS2 observations primarily based on the expectation that the detection and measure-

ment of their spectral features would benefit from the high throughput and spectral resolution of FORS2, and its reduced fringing at red wavelengths, relative to other instrumental options such as VIMOS. In particular, we expect that the main spectral emission and absorption features for galaxies at $0.8 < z < 1.6$ would appear at very red optical wavelengths, out to ~1 µm. Similarly, very faint Lyman break galaxies at $z \geq 4$, selected as B_{435}, V_{606}, and i_{775}–dropouts from the GOODS ACS photometry, also benefit greatly from the red throughput and higher spectral resolution of FORS2.

In practice, several categories of object selection criteria were used to ensure a sufficiently high density of target candidates on the sky to efficiently fill out multi-slit masks. Using ACS photometry in the AB magnitude system, these criteria were:

1. Primary catalog: $(i_{775}–z_{850}) > 0.6$ and $z_{850} < 24.5$. This should ensure redshifts $z \geq 0.7$ for ordinary early-type galaxies (whose strongest features are expected to be absorption lines), and higher redshifts for intrinsically bluer galaxies likely to have emission lines.
2. Secondary catalog: $0.45 < (i_{775}–z_{850}) < 0.6$ and $z_{850} < 24.5$.
3. Photometric-redshift sample: $1 < z_{phot} < 2$ and $z_{850} < 24.5$, using an early version of GOODS photometric redshifts like those described by Mobasher et al. (2004).
4. i_{775}-dropout and V_{606}–dropout Lyman break galaxy candidates, selected from the criteria of Dickinson et al. (2004a) and Giavalisco et al. (2004b), respectively.
5. A few miscellaneous objects, including host galaxies of supernovae detected in the GOODS ACS observing campaign.

When designing the masks, we generally tried to avoid observing targets that had already been observed in other redshift surveys of this field, namely, the K20 survey of Cimatti et al. (2002) and the survey of X-ray sources by Szokoly et al. (2004).

In the present spectroscopic catalog there are 303 targets, 114 meeting the primary selection criterion and 56 meeting the secondary selection criteria. The other targets belong to the remaining classes.

Observations and Data Reduction

The VLT/FORS2 spectroscopic observations were carried out in service mode during several nights in 2002 and 2003. In all cases the 300I grism was used as dispersing element without order-separating filter. This grism provides a scale of roughly 3.2Å/pixel. The nominal resolution of the configuration was $\Re=\lambda/\Delta\lambda=860$, which corresponds to about 9Å at 8000Å. The spatial scale of FORS2 was 0.126″/pixel, the slit width was always 1″. Dithering of the targets

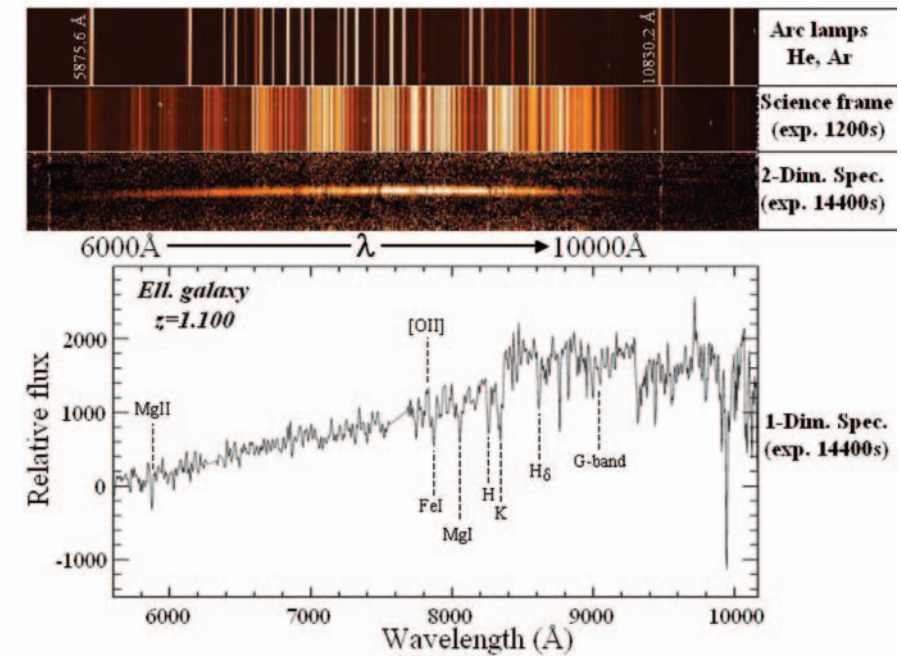

Figure 1: Typical FORS2 data products for an individual slit of the multi-object mask. From the top of the figure: the 2-D spectrum of the arc lines used for the wavelength calibration, a 2-D science exposure (1200 seconds), the final flat-fielded and sky-subtracted 2-D spectrum (co-addition of 12 exposures for a total of 4 h), and at the bottom the 1-D spectrum with the identification of the main absorption and emission lines (in this example an elliptical galaxy at z = 1.100, GDS J033217.46-275234.8).

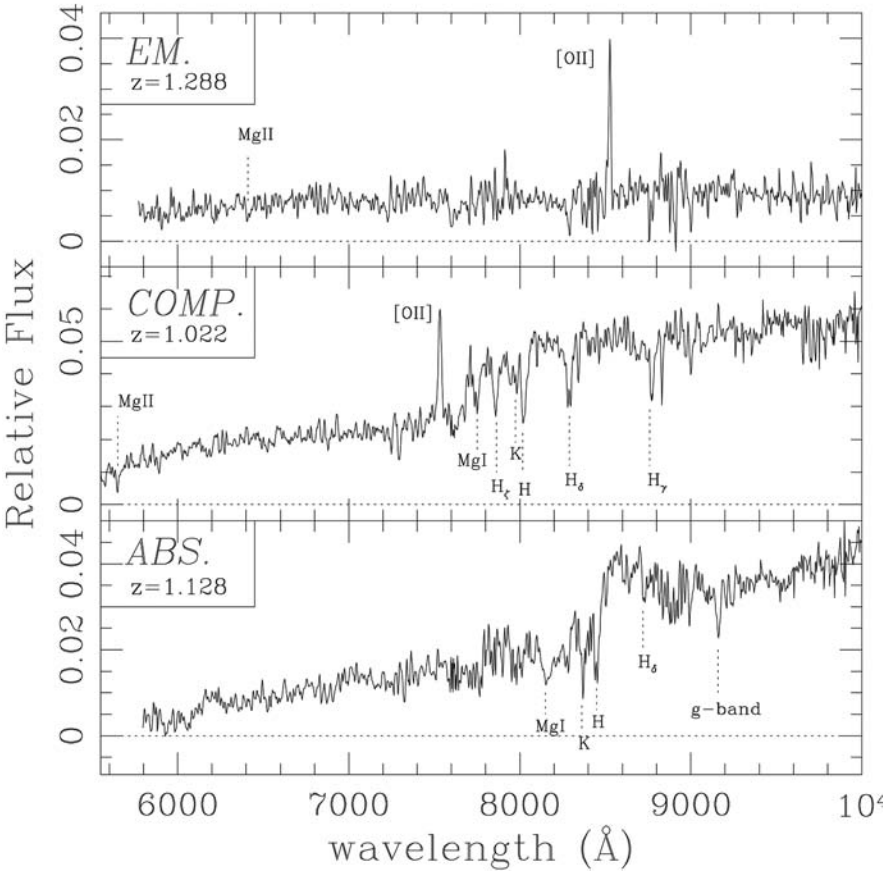

Figure 2: Three examples of objects classified as “em.” (emission-lines detected), “abs.” (absorption lines) and “comp.” (both emission and absorption lines detected).

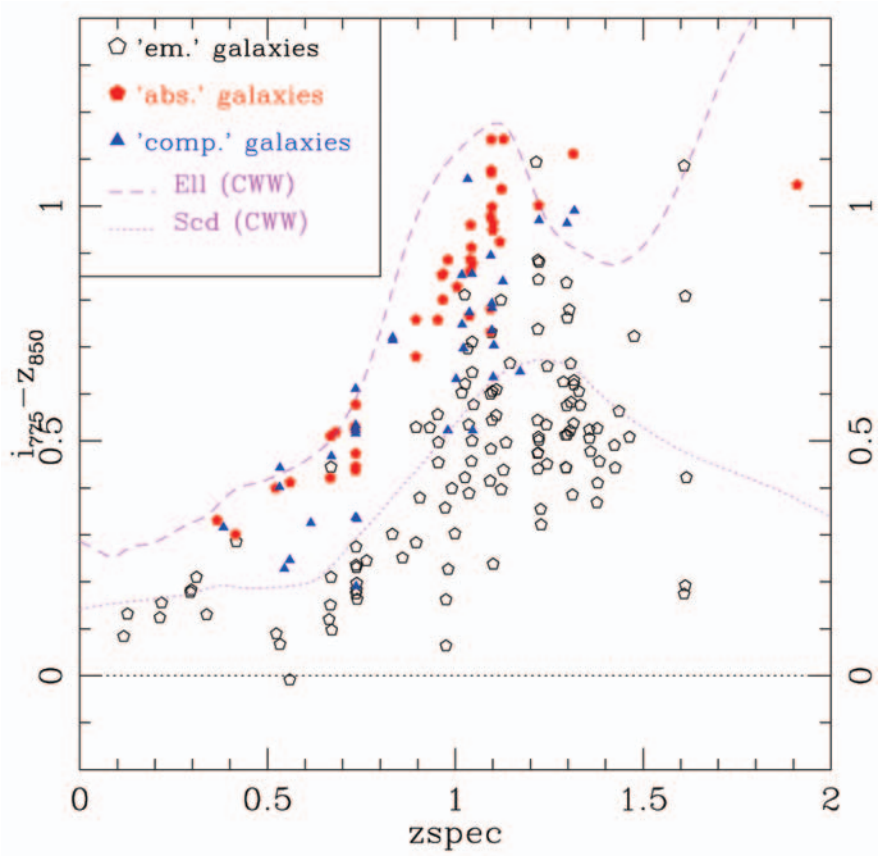

Figure 3: Color-redshift diagram of the spectroscopic sample. Only redshifts with quality flag "*A*" and "*B*" have been selected. Filled pentagons symbols are objects identified with absorption features only ("abs." sources), while open pentagons are objects showing only emission lines ("em." sources). The intermediate cases are shown by filled triangles ("comp." sources). The long-dashed line and the short dashed line show the colors of a non-evolving *L** elliptical galaxy and an Scd galaxy, respectively, estimated integrating the spectral templates of Coleman, Wu & Weedman (1980) through the ACS bandpasses.

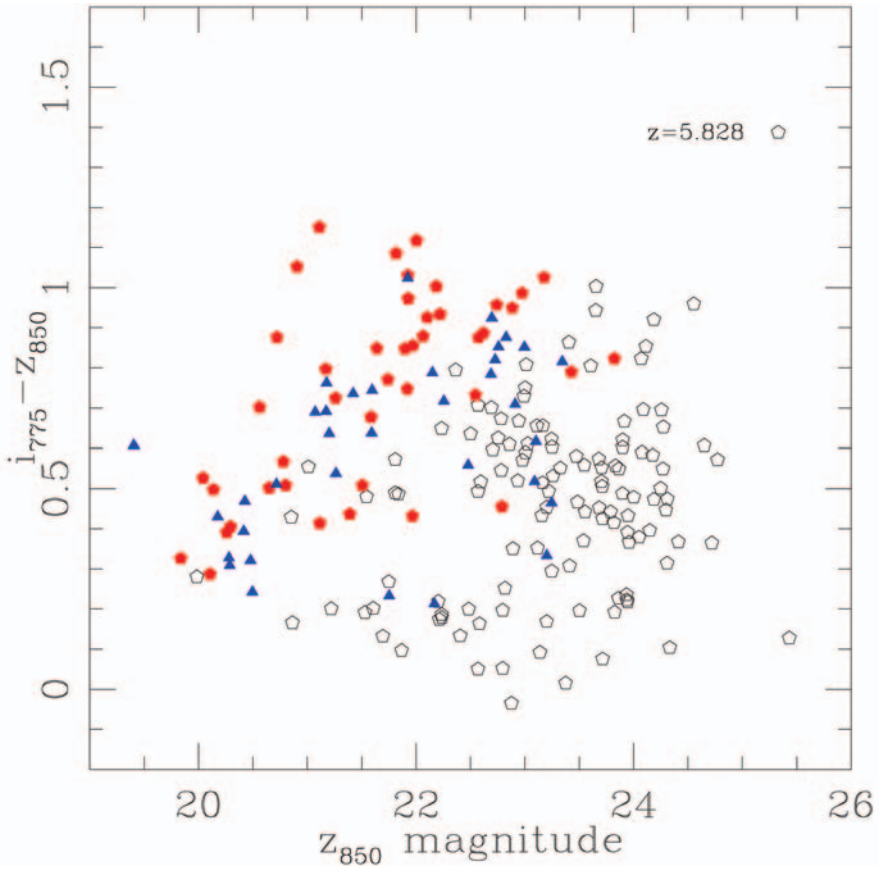

Figure 4: Color-magnitude diagram for the spectroscopic sample. Only redshifts with quality flag "*A*" and "*B*" have been selected. The symbols are the same as in Figure 3.

along the slits was applied in order to effectively improve the sky subtraction and the removal of CCD cosmetic defects.

399 spectra of 303 individual targets have been extracted and calibrated with a semi-automatic reduction tool that we have developed in the MIDAS environment using commands of the LONG and MOS contexts (Fig. 1). From the spectra we have been able to determine 234 redshifts. In the large majority of cases the redshift has been determined through the identification of prominent features of galaxy spectra: the 4000Å break, Ca H and K, *g*-band, Mg II 2798, Al II3584 in absorption and Ly-α, [O II]3727, [O III]5007, H_β, H_α in emission. The redshift estimation has been performed by cross-correlating the observed spectrum with templates of different spectral types (S0, Sa, Sb, Sc, Ell., Lyman Break, etc.), using the *rvsao* package in the IRAF environment. The redshift identifications are available at http://www.eso.org/science/goods/ and in Vanzella et al. (2004).

The objects have been classified in three categories (see Fig. 2) depending on the presence in the observed spectrum of emission line(s) (class *em.*), absorption-line(s) (*abs.*) or both (*comp.*). Eleven objects have been classified as stars. A quality flag has also been assigned to indicate "secure" redshift (flag *A*), "likely" (*B*) or "tentative" (*C*). In 38% of the cases the redshift is based only on one emission line, usually identified with [O II]3727 or Ly-α. In general these solo-emission line redshifts are classified as flag *C* or *B*. The presence of breaks, the absence of other spectral features in the observed spectral range and the broad band photometry are particularly important in the evaluation. The typical redshift uncertainty on the basis of internal and external comparisons, is estimated to be $\sigma_z \cong 0.001$ with a rate of "catastrophic" misidentifications at most few percent.

Diagnostic diagrams

Figures 3 and 4 show the color-redshift and the color-magnitude distributions for the spectroscopic sample. In Figure 3 the two populations of "emission-line" and "absorption-line" (typically elliptical) galaxies are clearly separated. The mean color of the "absorption-line" objects increases from $i_{775}–z_{850}$ = 0.46 ± 0.079 at $<z>$ = 0.6 to $i_{775}–z_{850}$ = 0.86 ± 0.18 at $<z>$ = 1.0, consistent with but increasingly bluer than the colors of a non-evolving *L** elliptical galaxy (estimated integrating the spectral templates of Coleman, Wu & Weedman (1980) through the ACS bandpasses).

The "emission-line" objects show in general a bluer $i_{775}–z_{850}$ color and a broader distribution than the "absorption-line" sources: $i_{775}–z_{850}$ = 0.16 ± 0.13 at $<z>$ = 0.6 and $i_{775}–z_{850}$ = 0.52 ± 0.21 at $<z>$ = 1.1. The broader distribution, with some of the

"emission-line" objects entering the color regime of the ellipticals, is possibly explained by dust obscuration, high metallicity or strong line emission in the z_{850} band.

Redshift distribution and Large Scale Structure

Figure 5 shows the redshift distribution of the objects observed in the present survey. The majority of the sources are at redshift of about one (the median of the redshift distribution is at 1.04), in agreement with the main criterion for the target selection (see Sect. 2). Table 1 shows the fraction of determined redshifts as a function of the spectral features identified, i.e. emission lines, absorption lines, emission & absorption lines, and no reliable spectral features (unclassified). There are 49 galaxies identified with absorption lines only (mainly Ca H and K) in the range of redshift between 0.4–1.3; an example is shown in Fig. 1. In 46% of the total sample we have measured emission lines (mainly [O II]3727), many of them entering the so-called "spectroscopic desert" up to z=1.61.

The main peaks in the redshift distribution are at z~0.73 (21 galaxies) and 1.1 (25 galaxies). Two concentrations at z~1.6 (with 5 galaxies at the mean redshift $<z> = 1.612 \pm 0.003$, see the two dimensional spectra in Fig. 6) and z~0.67 (9 galaxies) are also apparent. The presence in the CDF-S of large scale structure, (LSS) at z~0.73 and z~0.67 is already known (Cimatti et al. 2002, Gilli et al. 2003, Le Fevre et al. 2004). The peak at z~1.1 seems to be a new indication of large scale structure, of the 25 galaxies in the range $1.09< z <1.11$, 10 show emission lines, 9 are ellipticals and 6 are intermediate-type galaxies.

The significance of the LSS at z=1.61, which extends across a transverse size of ~ 5 Mpc in a wall-like pattern rather than a group structure, is confirmed by:

1. the observations of Gilli et al. (2003) who found a peak in the redshift distribution of X-ray sources at z=1.618 (5 galaxies) and measured a Poisson probability of $3.8\ 10^{-3}$ for a chance distribution;
2. three more galaxies at z=1.605,1.610,1.615 in the K20 survey (Cimatti et al. 2002).

High redshift galaxies

Three galaxies have been identified at redshifts larger than four: GDS J033240.01-274815.0 at z=5.828, the only i_{775}-dropout (see Sect. 2) actually targeted in the present observations, and two serendipitously-observed high redshift sources, GDS J033228.84-274132.7 and GDS J033228.94-274128.1, measured at z=4.800 and z=4.882, respectively. In the spectrum of GDS J033240.01-274815.0 the Ly-α line is clearly detected at z=5.828 and shows the blue cut–off characteristic of high–redshift Ly-α emitters and the Ly-α forest continuum break.

Figure 7 shows a peculiar system of three sources: two emission-line sources above (~1.5 arcsecond) and below (~3 arcsecond) the main galaxy GDS J033228.88-274129.3, clearly visible in the ACS color image and in the two dimensional spectrum. The same target has been observed in two different masks adopting the same orientation of the slits. The total exposure time is ≅43 ks. The extracted one dimensional spectra are shown in the right side of Fig. 7.

The main galaxy GDS J033228.88-274129.3 has a redshift z=0.733 with both emission and absorption lines measured (quality flag "A"): [O II]3727, MgI, Ca H and K, *g*-band, etc. The bottom object (GDS J033228.84-274132.7) shows a solo-emission line at 7052Å (see the 1D spectrum), and is not detected in the ACS *B*-band, we interpret this line as Ly-α at z=4.800 with quality "*C*".

The source above GDS J033228.88-274129.3 is most probably a Ly-α emitter at redshift

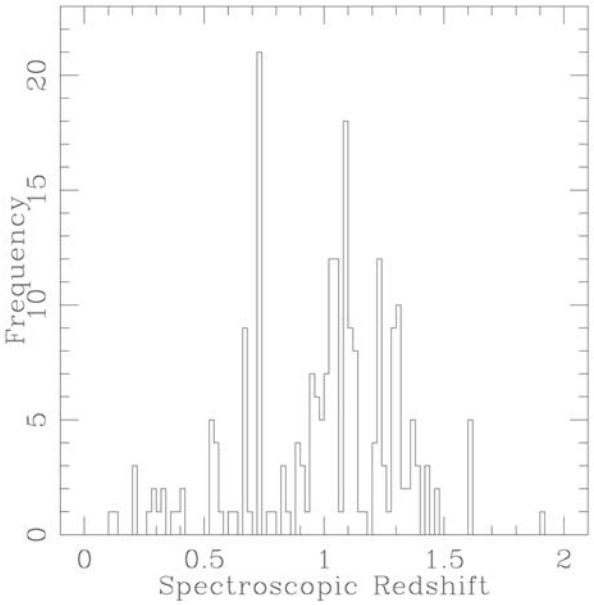

Figure 5: Redshift distribution for the spectroscopic sample with quality *A, B* and *C* (23 redshift determinations out of 224 have quality *C*). Three objects at z>4 are not shown in the histogram.

Table 1: Fractions of sources with different spectral features.

Spectral class	z_{mean}	z_{min}	z_{max}	Fraction
emission	1.131	0.117	5.828	46%
absorption	0.950	0.366	1.910	16%
em. & abs.	0.897	0.382	1.317	12%
stars	0.000	0.000	0.000	4%
unclassified	–	–	–	22%

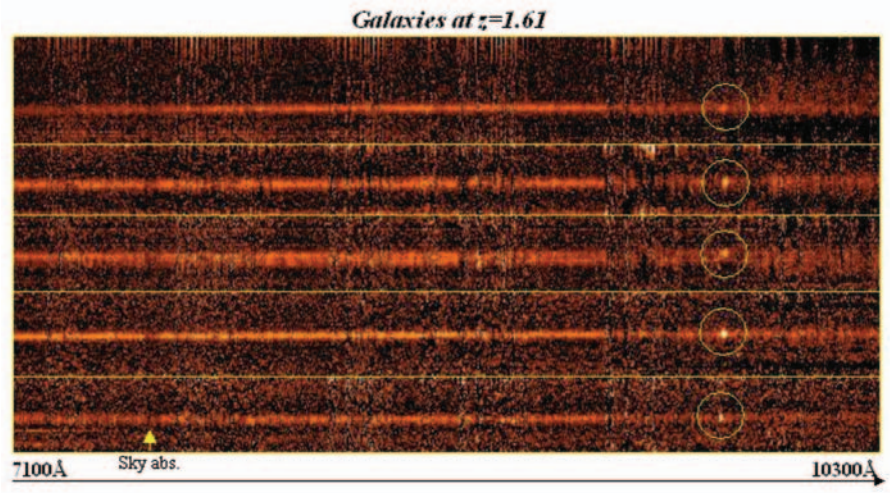

Figure 6: Two dimensional spectra of 5 galaxies at z=1.61. The [O II]3727 emission line is marked with a circle at 9727.5Å. The absorption sky feature (~7600Å, *A* band) is indicated with an arrow. It is worth noting the optimal red sensitivity of FORS2.

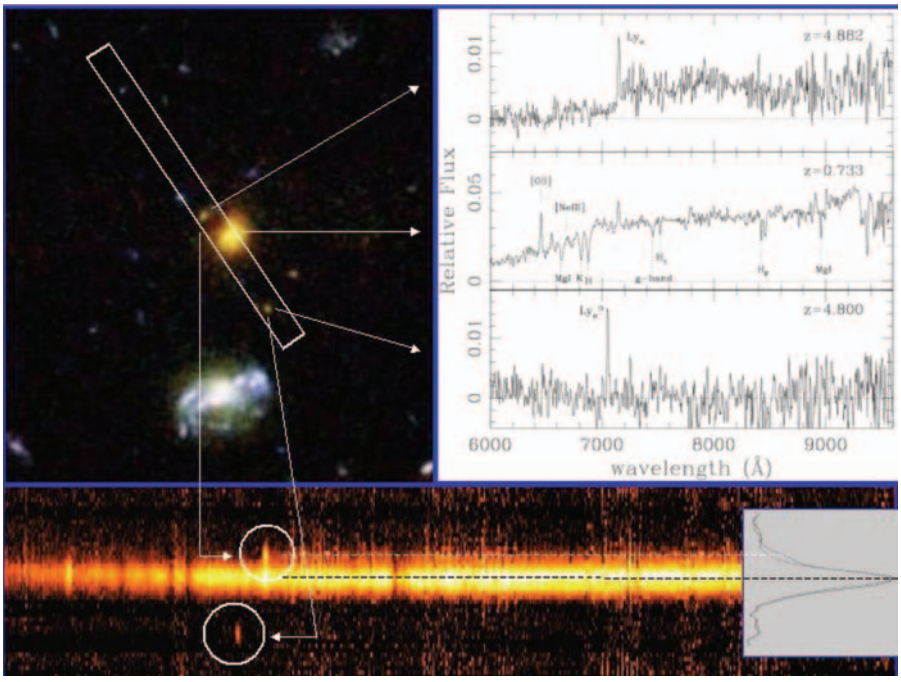

Figure 7: Simultaneous spectrum of three sources in the slit. On the right of the figure, the 1D spectra of the *z*=0.733 main galaxy GDS J033228.88-274129.3, the single emission line ~3 arcsecond below (GDS J033228.84-274132.7) and the object ~1.5 arcsecond above are shown. The left-hand panel shows the ACS color image, 5 arcsec on a side. North is up, east is to the left. The bottom panel shows the 2D spectrum, with the spatial profile obtained by collapsing 80 columns (256 Å), centered at 7150 Å, shown to the right. Candidate serendipitous Ly-α emission lines are clearly marked. The object above the target source shows faint continuum redward of the emission line.

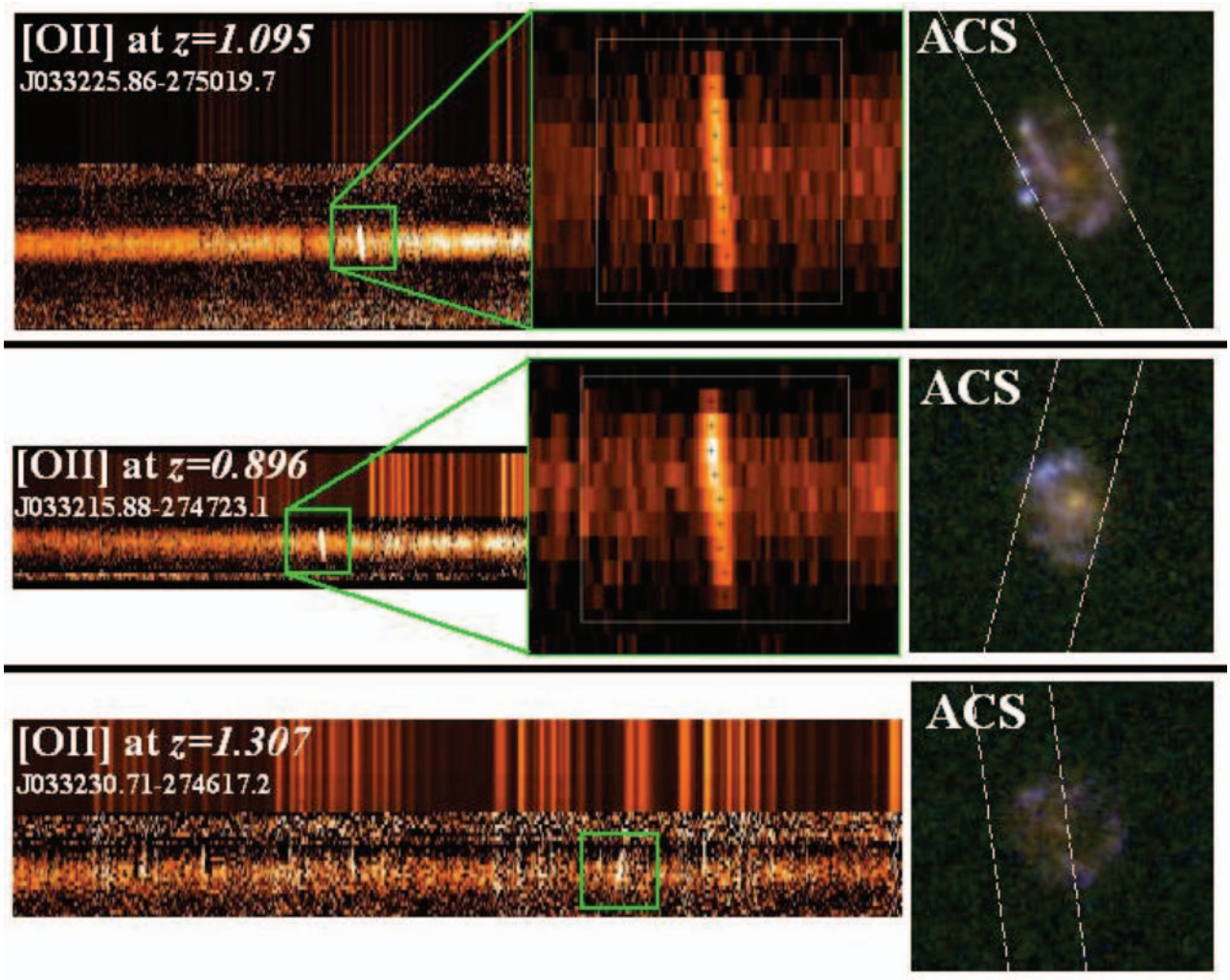

Figure 8: Three examples of tilted [O II]3727 emission line at redshift around 1. The two dimensional FORS2 spectra are shown (object and sky lines). In the first two spectra (top and middle) a zoom of the [O II]3727 emission line is shown (the white rectangle underlines the region where the Gaussian fit has been performed to derive the line peak, small black crosses), in the bottom spectrum the line is too faint to calculate a reliable peak (this object has been serendipitously-identified). In the right side of the spectra the ACS images of the galaxies and the slit orientations are shown.

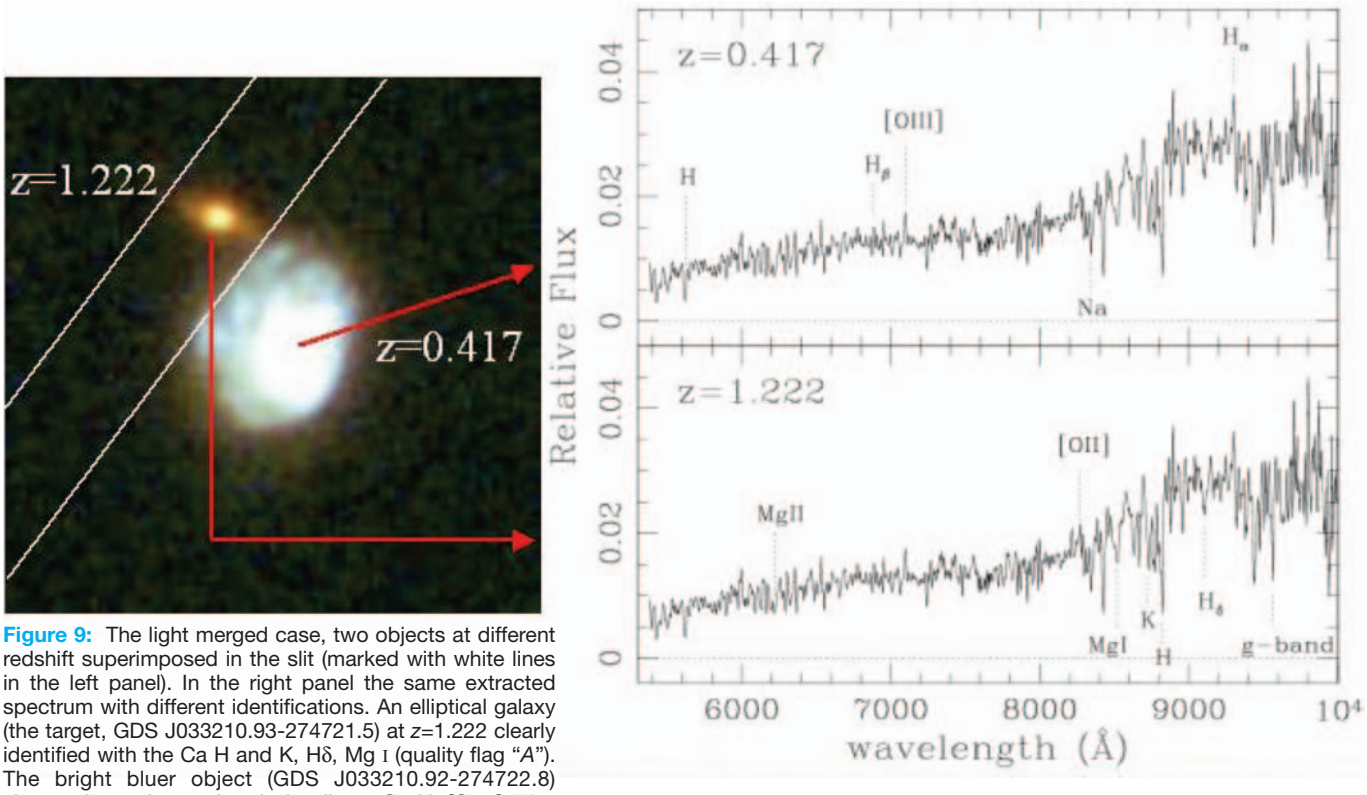

Figure 9: The light merged case, two objects at different redshift superimposed in the slit (marked with white lines in the left panel). In the right panel the same extracted spectrum with different identifications. An elliptical galaxy (the target, GDS J033210.93-274721.5) at z=1.222 clearly identified with the Ca H and K, Hδ, Mg I (quality flag "*A*"). The bright bluer object (GDS J033210.92-274722.8) shows absorption and emission lines: Ca H, [O III]5007, Na, Hα at z=0.417 (quality flag "*B*"). The Ca K is contaminated by the sky line ~5577Å.

z=4.882 (quality "B"). The spectrum has been extracted subtracting the contamination of the tail of the main galaxy. After the subtraction the shape of the spectrum shows the blue cut–off and the Ly-α forest continuum break, typical of the LBGs.

Dynamical masses of galaxies at $z \sim 1$

Three galaxies, GDS J033215.88-274723.1, GDS J033225.86-275019.7 and GDS J033230.71-274617.2, at redshift z=0.896, 1.095 and z=1.307, respectively, show a spatially resolved [O II]3727 line (Fig. 8) with a characteristic "tilt", indicative of a high rotation velocity. The measured velocity increases with increasing distance from the center of the objects reaching a value of the order of and greater than 400 km/s at the extremes. Assuming that the observed velocity structure is due to dynamically-relaxed rotation, then it is possible to estimate the dynamical mass for the three galaxies, which turns out to be in the range 1.5–3.1 $10^{11}/sin^2\ (i)$ $M_\odot$. The estimates should be considered a lower limit to the total dynamical mass because more external parts of the rotating structure might have a lower surface brightness and remain undetected.

GDS J033210.93-274721.5: a spectrum contaminated by a nearby galaxy

The spectrum of the galaxy GDS J033210.93-274721.5 simultaneously shows features corresponding to the redshifts z=1.222 and z=0.417 (Fig. 9). The origin of the overlap is the presence of a nearby galaxy (z_{850}=19.98, GDS J033210.92-274722.8) offset by 1.3 arcsecond with a redshift z=0.417. Light from the brighter z=0.417 galaxy contaminates the spectrum of the fainter (z_{850}=22.19), higher redshift galaxy GDS J033210.93-274721.5 (see Fig. 9). Such cases may represent a problem and a source of error in large spectroscopic surveys, which require highly automated data processing. A possible solution is to evaluate *a priori* on the basis of imaging what are the cases of light contamination requiring a "special" reduction. Alternatively, color-redshift diagrams (such as Fig. 3), a comparison of spectroscopic and photometric redshifts or similar diagnostics are required to carry out the necessary data quality control and single out possible misidentifications.

References

Abraham, R., G., van den Bergh, S., Glazebrook, K., Ellis, R., S., Santiago, B., X., Surma, P., Griffiths, R., E., 1996, ApJ, 107, 1

Cimatti, A., Mignoli, M., Daddi, E., et al. 2002, A&A, 392, 395

Coleman, G., D., Wu, C.-C., & Weedman, D., W., 1980, ApJS, 43, 393

Dickinson et al. 2003, in the proceedings of the ESO/USM Workshop "The Mass of Galaxies at Low and High Redshift" (Venice, Italy, October 2001), eds. R. Bender and A. Renzini, astro-ph/0204213

Dickinson, M., et al., 2004, ApJ, 99, 122

Giavalisco, M., et al. 2004, ApJ, 600, L93

Giavalisco, M., Dickinson, M., Ferguson, H. C., Ravindranath, S., Kretchmer, C., Moustakas, L. A., Madau, P., Fall, S. M., Gardner, Jonathan P., Livio, M., Papovich, C., Renzini, A., Spinrad, H., Stern, D., Riess, A., 2004, ApJ, 600, 103

Gilli, R., Cimatti, A., Daddi, E., Hasinger, G., Rosati, P., Szokoly, G., Tozzi, P., Bergeron, J., Borgani, S., Giacconi, R., Kewley, L., Mainieri, V., Mignoli, M., Nonino, M., Norman, C., Wang, J., Zamorani, G., Zheng, W., Zirm, A., 2003, ApJ, 592, 721

Le Fevre, O., Vettolani, G., Paltani, S., Tresse, L., Zamorani, G., Le Brun, V., Moreau, C., and the VIMOS VLT Deep Survey team, submitted to A&A, (astro-ph/0403628)

Mobasher, B., Idzi, R., Benítez, N., Cimatti, A., Cristiani, S., Daddi, E., Dahlen, T., Dickinson, M., et al., 2004, ApJ, 600, 167

Renzini et al. 2002, in the proceedings of the ESO/USM Workshop "The Mass of Galaxies at Low and High Redshift" (Venice, Italy, October 2001), eds. R. Bender and A. Renzini

Riess, A.G.,2 Strolger, L.-G., Tonry, J., Casertano, S., Ferguson, H.C., et al., 2004, ApJ, 607, 665

Steidel, C.C., Adelberger, K.L., Giavalisco, M., Dickinson, M., Pettini, M., 1999, ApJ, 519, 1

Szokoly, G., P., Bergeron, J., Hasinger, G., Lehmann, I., Kewley, L., Mainieri, V., Nonino, M., Rosati, P., Giacconi, R., Gilli, R., Gilmozzi, R., Norman, C., Romaniello, M., Schreier, E., Tozzi, P., Wang, J., X., Zheng, W., Zirm, A., 2004, (astro-ph/0312324)

Vanzella, E., Cristiani, S., Dickinson, M., et al. astro-ph/0406591